

Ignition and Front Propagation in Polymer Electrolyte Membrane Fuel Cells

J. B. Benziger,* E.-S. Chia, Y. De Decker, and I. G. Kevrekidis

Department of Chemical Engineering, Princeton University, Princeton, New Jersey 08544

Received: September 1, 2006; In Final Form: November 10, 2006

Water produced in a polymer electrolyte membrane (PEM) fuel cell enhances membrane proton conductivity; this positive feedback loop can lead to current ignition. Gas-phase convection and membrane diffusion of water coupled with water production in a simplified two-dimensional PEM fuel cell leads to localized ignition and current density front propagation in the cell. Co-current gas flow in the anode and cathode channels causes ignition at the cell outlet, and membrane diffusion causes the front to slowly propagate toward the inlet; counter-current flow in the anode and cathode channels causes ignition in the interior of the cell, with the current density fronts subsequently spreading toward both inlets. The basic chemistry and physics of the spatiotemporal nonlinear dynamics of the two-dimensional fuel cell current can be captured by extending a simple one-dimensional stirred tank reactor model to a “tanks-in-series” model.

Introduction

Fuel cells constitute a reliable and environmentally friendly alternative energy source.^{1,2} Polymer electrolyte membrane (PEM) fuel cells are viewed as the most promising for automotive applications. The basic operation of a PEM fuel cell is illustrated in Figure 1. Hydrogen molecules dissociatively adsorb at the anode and are oxidized to protons. Electrons travel through an external load resistance to the cathode, and protons diffuse through the PEM under an electrochemical gradient to the cathode. Oxygen molecules adsorb at the cathode, are reduced, and react with the protons to produce water. The product water is absorbed into the PEM or evaporates into the gas streams at the anode and cathode. Water management is a key engineering challenge for the commercial deployment of PEM fuel cells; the hydration state of the membrane–electrode assembly must be controlled for good operation.

Beyond steady-state operation, understanding of fuel cell startup and transient dynamic behavior is crucial to their use in *variable load* automotive applications.^{3,4} These transient dynamics are intensely nonlinear because of a positive feedback loop: we recently demonstrated that water generated in a one-dimensional, stirred tank reactor (STR), polymer electrolyte membrane (PEM) fuel cell *increases* proton transport exponentially, which “ignites” the current.^{5,6} The positive feedback loop, driven by an exponential increase in the rate of reaction, is characteristic of autocatalytic nonlinear dynamic systems.^{7,8} Such a classical nonlinear reacting dynamical system results from the coupling of mass transport with an exothermic chemical reaction. There, a product of the reaction (heat) enhances the reaction rate by raising the temperature.^{9–12} In autohumidified PEM fuel cells, the positive feedback between membrane water activity and proton conductivity is known to cause steady-state multiplicity.^{13,14}

Here we present *spatiotemporal* nonlinear dynamic phenomena in a two-dimensional PEM fuel cell reactor (current ignition and current density front propagation along flow channels). PEM fuel cells typically have flow channels that distribute the fuel (hydrogen) across the anode and oxidizer (oxygen) across the

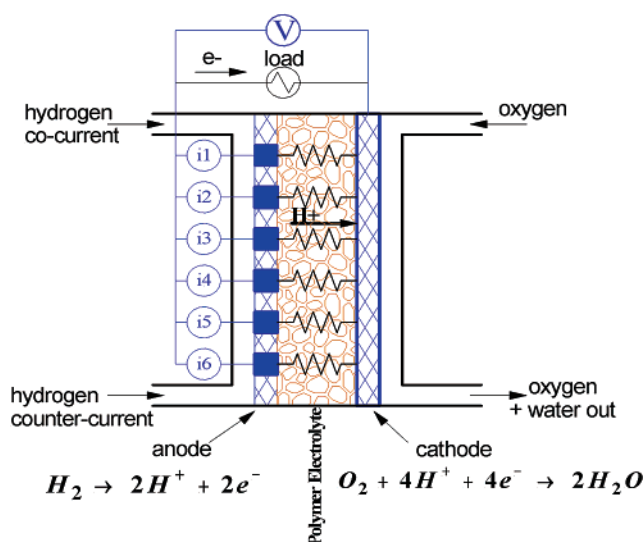


Figure 1. Schematic of a hydrogen–oxygen PEM fuel cell including internal and external equivalent circuit elements.

cathode (Figure 1).¹⁵ Longitudinal water gradients in the membrane can produce a sharp current density front that propagates in time along the channel.^{16,17} To design and control variable load, *dynamic* fuel cell operation, the mechanism underlying such dynamics must be understood.

Experimental Section

Figure 2 shows a photograph of a simplified fuel cell with a segmented anode that permits current profile measurements. The equivalent circuit for the segmented anode fuel cell is shown in Figure 1. The anode and cathode flow channels are parallel, separated by a membrane–electrode assembly. The current through each electrode segment of the anode and the voltage drop across the external load resistor are recorded as a function of time. The cell operates at atmospheric pressure; the flow rates of hydrogen at the anode and oxygen at the cathode are maintained with mass flow controllers. The external load resistance is a 10 turn potentiometer that can be adjusted between 0 and 20 Ω .

* Corresponding author. E-mail: benziger@princeton.edu.

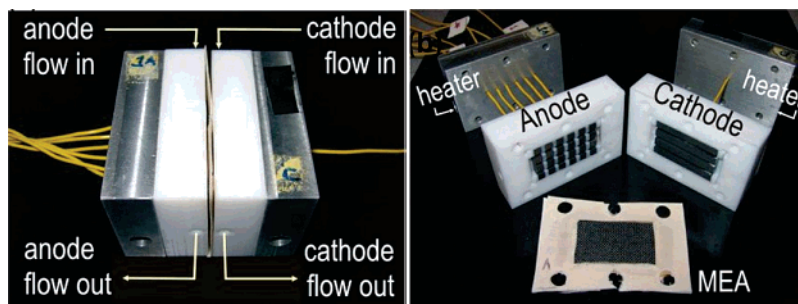


Figure 2. Segmented anode fuel cell. The anode electrode was broken into six individual elements separated by Teflon spacers. Current through each element was measured independently. A membrane–electrode assembly employing two E-TEK electrodes with carbon supported Pt catalyst and a Nafion 115 membrane was placed between anode and cathode.

The fuel cell had three parallel flow channels 1.6 mm square by 30 cm long. The anode was constructed of alternating pieces of Teflon and graphite, dividing it into 6 separate segments. The cathode had three parallel flow channels machined out of a single piece of graphite. The flow channel pieces were fitted into Teflon blocks with electrical leads coming out the back. The leads were connected through the potentiometer. Electrical probe clips were attached at various points for current and voltage measurements.

An MEA was placed between the cathode and anode and sealed. We made our own MEA of a Nafion 115 membrane pressed between two E-tek electrodes (these consist of a carbon cloth coated on one side with a Pt/C catalyst). The catalyst weight loading was 0.4 mg Pt/cm². The electrodes were brushed with solubilized Nafion solution to a loading of ~ 1 mg Nafion/cm² before placing the membrane between them.¹⁸ The assembly was hot pressed at 130 °C and 10 MPa. The Nafion membrane extended beyond the carbon cloth by ~ 3 mm and was pressed between silicon rubber sheet gaskets that sealed the MEA from the sides.

The fuel cell is placed between two temperature-controlled aluminum blocks. There are six segments to the fuel cell, each with an active area of 0.5 cm². The fuel cell was preconditioned with a 20 Ω load at 60 °C and flow rates of 3.5 sccm H₂ at the anode and O₂ at the cathode for 8–12 h. The current in each segment was < 1 mA after preconditioning (extinction). The external load was then reduced to 0.25 Ω keeping temperature and flow rates fixed.

Results

The gas flows at the anode and cathode can be either co-current or counter-current. In Figure 3, we show the current in each anode segment with counter-current flow at 60 °C. The current in each segment remained at < 1 mA for more than 4 h, at which time 100 μ L of water was injected into the anode feed stream. The current response for each segment after the water injection is shown. The injection of the water “ignited” the fuel cell current. Before water injection the resistance of the dry membrane for proton conduction was very high (> 10 k $\Omega \cdot \text{cm}^{-2}$), limiting the current and hence the water production. After water was injected into the anode gas stream some of it was absorbed into the membrane, decreasing the membrane resistance to ~ 1 $\Omega \text{ cm}^{-2}$; this increased the currents to ~ 100 mA and made the fuel cell self-sustaining.

To identify the location of current ignition in the flow channels and the time required to ignite the current through gradual water accumulation in the membrane, the fuel cell was extinguished as described above (60 °C, 20 Ω load resistance). After current extinction the temperature was then reduced to 25 °C, decreasing the water removal and the load resistance

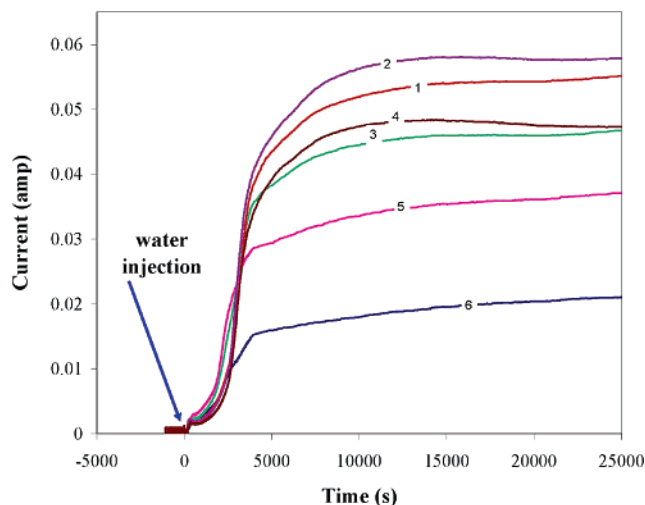


Figure 3. Fuel cell ignition by water injection. The fuel cell was preconditioned so as to dry the membrane; the current in each segment of the anode was then < 1 mA. The gas flows were counter-current, the temperature was 25 °C, and the load resistance was 0.25 Ω . At $t = 0$, 100 μ L of water was injected into the anode (hydrogen) feed. After the water was absorbed into the membrane, the fuel cell currents rose dramatically (ignited) and remained so. The numbers refer to the currents in the segments in order: 1 is at the anode inlet, and 6 is at the anode outlet.

reduced to 0.25 Ω , increasing the water production. Current and voltage were recorded every 10 s for a period of 20 h after these changes. For the measurements reported here, the fuel cell was placed with the flow channels running vertically. Co-current measurements were made with both H₂ and O₂ flows going from top to bottom; for counter-current measurements, the oxygen flow went from top to bottom and the hydrogen flow from bottom to top.

The current distributions along the flow channels as functions of time are shown in Figure 4a for co-current flow and 4b for counter-current flow. An induction period was required before any significant current was measured; the length of this induction period depended on how dry the fuel cell membrane was before startup (i.e., before reducing the load resistance.) Typical induction periods were about 1 h but could be as long as 4–5 h. For co-current flow (Figure 4a), ignition first occurred at the outlet of the fuel cell; the current in anode element 6, near the outlet, rose from < 1 mA to ~ 100 mA over a period of 5 min. A current ignition front then propagated from element 6 to element 1 over a period of 15–20 min; as the current front propagated toward the entrance of the flow channels, the current at the exits of the flow channels dropped. With counter-current flow ignition first occurred at element 3, at the interior of the flow channel (Figure 4b). From the center, the ignition fronts

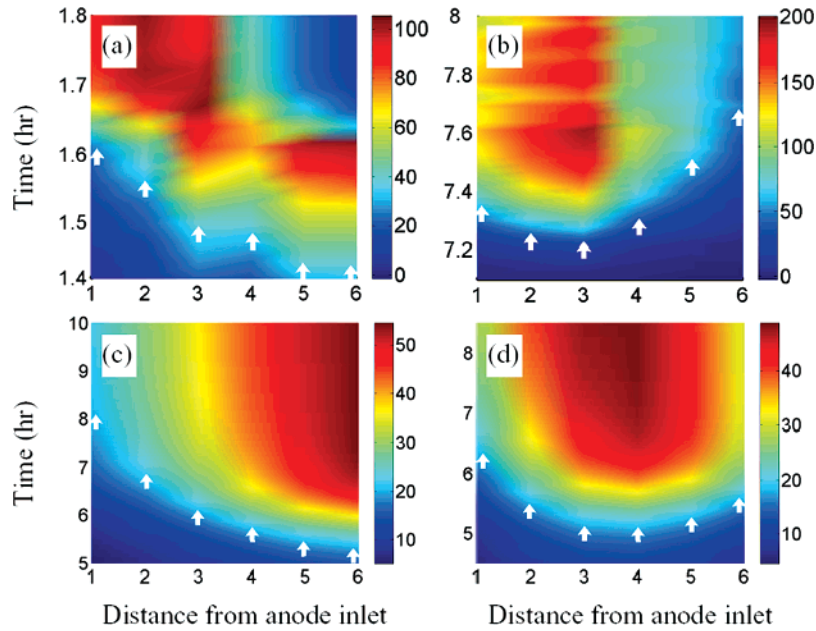


Figure 4. Comparison of the experimental and computed currents for co-current and counter-current flow of hydrogen and oxygen in a segmented anode PEM fuel cell. The color scale is for current through each anode segment in milliamperes. (a) Experimental co-current; (b) experimental counter-current; (c) computed co-current; (d) computed counter-current. For the simulations, the flow rate for H₂ and O₂ is 3.5 and 6.5 mL min⁻¹, respectively, and $k_m = 3 \times 10^{-6}$ mol s⁻¹.

“fanned” outward, but the highest current always occurred in the center of the flow channel. The induction period was also longer with counter-current flow than with co-current flow. The long-term, total steady-state current was roughly double for counter-current (as opposed to co-current) flow.

Discussion

We have been able to capture the basic physics of ignition dynamics in one dimension with a simple *lumped* parameter STR model;^{13,14} to capture *localized* ignition and spatiotemporal front propagation, the model is extended to a series of differential elements as “tanks-in-series”. The key features of the model are the water inventory in the polymer electrolyte, the transverse proton conductivity from the anode to the cathode, and the longitudinal water transport through the membrane. Water sorbed into the polymer ionizes sulfonic acid groups, facilitating proton transport; water sorption by the PEM is limited by the total number of sulfonic acid groups in the membrane. Water is sorbed into, or desorbed from, the membrane depending on the balance between water evaporating into the gas flow channels and water produced by the fuel cell. The multilayered membrane–electrode assembly in PEM fuel cells results in complex intra- and interlayer transport processes. Because the flow channels are much longer than the membrane thickness (5 cm vs 0.0125 cm), we make the simplifying assumption that water activity in the membrane is in local equilibrium with water activity in the gas flow channel above it, and the only gradients are longitudinal *along* the channel.

The water balance in each differential element, j , of the membrane is given by eq 1 for co-current gas flow ($j = 1$ to 6; $j = 0$ and $j = 7$ denote the anode inlet and outlet, respectively; the counter-current case easily follows); the inventory is balanced by water produced ($1/2$ the proton current), water convected in the gas flow, and longitudinal water diffusion (described by a lumped mass transfer coefficient between differential elements). Equation 2 is an empirical fit to the number of water molecules associated with each sulfonic acid

group, λ , as a function of water activity a_w in a Nafion 115 membrane.¹⁹

$$\left[N_{\text{SO}_3} \frac{d\lambda(j)}{da_w(j)} + (V_A + V_C) \frac{P_w^0}{RT} \right] \frac{d[a_w(j)]}{dt} = \frac{i(j)}{2F} + [F_A(j-1) + F_C(j-1)]P_w(j-1) - [F_A(j) + F_C(j)]P_w(j) + k_m[a_w(j+1) + a_w(j-1) - 2a_w(j)] \quad (1)$$

$$\lambda(j) = 14.9a_w(j) - 44.7a_w^2(j) + 70a_w^3(j) - 26.5a_w^4(j) - 0.446a_w^5(j) \quad (2)$$

We assume that the total gas pressure P_{tot} is fixed, and the local water activity in the membrane is in equilibrium with the local water partial pressure, that is, $P_w(j) = a_w(j)P_w^0$ and $P_{\text{H}_2}(j) = P_{\text{O}_2}(j) = P_{\text{tot}} - P_w(j)$; P_w^0 is the water vapor pressure at this temperature. The molar flow rates change along the flow channel as water is formed; the molar flows are given by $F_A(j) = F_A(j-1) - i(j)/4F$ and $F_C(j) = F_C(j-1)$; the subscript A(C) corresponds to the anode (cathode), $i(j)$ is the local current, and F is the Faraday constant. Last, we assume that the local potential $V_{\text{FC}}(j)$ between the anode and cathode is dictated by the thermodynamic driving force as in eq 3. This neglects interfacial potential drops and mass transport limitations, which results in the predicted currents being about 20% larger than those found in real fuel cells.

$$V_{\text{FC}}(j) = 1.23 + \frac{RT}{4F} \ln \left[\frac{P_{\text{H}_2}^2(j) P_{\text{O}_2}(j)}{P_{\text{atm}}^3 a_w^2(j)} \right] \quad [\text{V}] \quad (3)$$

On the basis of the equivalent electrical circuit, the differential elements are electrically connected *in parallel* to each other. The voltage across the external load resistance thus depends on the total current produced by all elements; the local current is given by eq 4. The local membrane resistance, $R_M(j)$, depends on the local water content in the membrane. For a Nafion 115

membrane employed in this fuel cell, the membrane resistance as a function of water activity is given by eq 5.¹⁹

$$i(j) = \frac{V_{\text{FC}}(j) - R_{\text{L}} \sum_{k \neq j} i(k)}{R_{\text{M}}(j) + R_{\text{L}}} \quad [\text{A}] \quad (4)$$

$$R_{\text{M}}(j) = 5 \times 10^5 \exp[-14a_{\text{w}}^{0.2}(j)] \quad [\Omega] \quad (5)$$

In a *single*, differential PEM fuel cell, ignition occurs when the initial water content in the membrane is sufficient for water production to exceed water removal by convection. Here ignition will occur when (and where!) the water production exceeds water removal, that is, when (and where) the right-hand side of eq 1 becomes greater than zero. Water production depends on the load resistance and the membrane resistance. A dry membrane has a resistance of $500 \text{ k}\Omega \text{ cm}^{-2}$, limiting the current density to a maximum of $2.4 \mu\text{A cm}^{-2}$. According to eq 1 the feed flow rates would have to be $<0.1 \text{ mL h}^{-1}$ at a fuel cell temperature of $60 \text{ }^\circ\text{C}$ for water production to be greater than water removal and ignite the fuel cell. Absorption of $10 \mu\text{L cm}^{-2}$ of water into the membrane reduces its resistance to $10 \Omega \text{ cm}^{-2}$ and the maximum current density is 100 mA cm^{-2} , sufficient for water production to exceed water removal and the fuel cell to ignite as shown in Figure 3. (The actual amount of water that must be injected for ignition is greater than $10 \mu\text{L cm}^{-2}$ because only a fraction of the injected water is sorbed into the membrane; a significant fraction of the water injected is convected out of the fuel cell with the gas flow before it is sorbed into the membrane).

The key elements that account for ignition are (1) an exponential dependence of proton conductivity in the PEM with membrane water content and (2) the dynamics of water uptake into the PEM. The location of ignition and front propagation are consequences of (1) convection of water produced toward the cell downstream, where it can accumulate, and (2) diffusion of water upstream through the polymer membrane. Figure 4c and d shows the *simulated* current profiles for co-current and counter-current flow with $T = 47 \text{ }^\circ\text{C}$, $R_{\text{L}} = 5 \Omega$. The model captures both the ignition and the front propagation. The model is only semiquantitative because it neglects finite water mass transfer rates into the membrane and from the membrane into the gas phases. It also neglects the effects of condensing liquid water, hindering gas transport from the flow channels to the membrane/electrode interface. More detailed models that incorporate these effects can give quantitative fits to experimental results; yet the added complexity does not significantly enhance physical understanding. The experimental time scale for ignition in co-current flow is shorter than the simulation predicts. This time difference is due to the level of dryness of the membrane at time zero. We did not always get the membrane to the same level of dryness. If there is slightly more water present at time zero, then ignition occurs sooner.

The model simulations were carried out at a slightly higher temperature and load resistance than the experiments because we had to choose conditions for the model where liquid water would not condense. Our present simple model does not account for two-phase flow. By increasing the temperature water vapor convection is increased, and increasing the load resistance decreases the water produced. The simulated conditions are as close as we could get to the experimental conditions with a balance of water production and water removal without liquid condensation. Higher load resistances in the simulations resulted in currents lower than those observed experimentally. If the load

resistance in the simulation was the same as that in the experiment, then the simulation would have a higher current than the experiment.

For co-current flow the water produced upstream is conducted toward the outlet, where it slowly accumulates in the membrane; when the water content increases to the point where the local membrane resistance becomes comparable to the external load resistance the current starts increasing rapidly, hydrating the membrane and causing ignition at the outlet of the flow channel. Upon ignition, the water activity in the membrane approaches unity. Water is then transported upstream through diffusion in the membrane itself, causing upstream propagation of the ignition. The model did not capture the observed eventual decrease in the downstream current, after the ignition propagated to the inlet of the fuel cell. This decrease is due to *condensing water* accumulating in the cathode, inhibiting oxygen transfer to the catalyst and reducing the current. In counter-current flow, water formed at the cathode is convected toward the anode inlet in the cathode flow channel. Water is also transported *across the membrane* to the anode, where it is convected toward the anode outlet. Water accumulates fastest toward the middle of the flow channels, resulting in an interior ignition point. The ratio of the flow rates between the anode and cathode affects the ignition point location; a relative increase of the anode flow rate shifts the ignition toward the anode outlet. After ignition, water starts to accumulate locally in the membrane. The transport of water *through* the membrane from high concentration at the middle of the flow channel toward the outlets results in the “fanning out” of the ignition fronts.

Liquid water was observed leaving the flow channels 30–40 min after ignition. Ignition takes the fuel cell from very low water activity to water activity of unity. Further water production does not change the water activity but leads to condensation of liquid water in the flow channels. Gravity plays a key role in how such liquid water moves through the flow channels; the operation changes dramatically if gas flow in the channel is counter to gravity-driven liquid water flow. When the fuel cell was vertical, gravity caused the liquid to drain and permitted good access for the reactants from the flow channels to the electrode/electrolyte interface. When the fuel cell was horizontal, the initial ignition phenomena were similar to those reported in Figure 3 after ignition; however, large fluctuations in the local current density appear to correlate with water droplets exiting the cell. In the horizontal orientation, liquid water condensing in the flow channels could partially block flow. The liquid drops were pushed along the flow channels by the flowing gas, but in an irregular fashion that gave rise to large fluctuations in the local current density. Transport of liquid water in the flow channels is not accounted for at our level of modeling. The model can thus capture ignition and front propagation, but will break down at longer times when liquid water floods the cathode gas diffusion layer (GDL) and starts entering the flow channels.

Conclusions

We have demonstrated how the water exponentially increases proton conductivity in polymer electrolyte membranes leading to ignition of the current in PEM fuel cells. Water can be injected to a fuel cell to ignite the current, just like a match can be struck to ignite a flame. Transport of water laterally, coupled with the exponential increase in proton conductivity, produces current fronts that propagate along flow channels, just like flame fronts. The positive feedback loop between water production and increased proton conductivity of the electrolyte membrane in PEM fuel cells is analogous to exothermic chemical reaction

ignition and flame propagation; “water fans the flame” in PEM fuel cells! Front propagation depends on flow configurations creating different front ignition and propagation patterns. Understanding the parametric dependence and time scales of these phenomena is a vital component of fuel cell design, non-steady-state operation, and control.

Acknowledgment. We thank the National Science Foundation (CTS-0354279 and DMR-0213707) for support of this work. E.C. thanks the Princeton University Program in Plasma Science and Technology, and U.S. Department of Energy Contract No. DE-AC02-76-CHO-3073 for fellowship support. Y.D. thanks the Belgian American Educational Foundation for financial support.

Nomenclature

$a_{w(j)}$ = water activity in reactor element j
 F = Faraday’s constant (96 458 C/mol)
 $F_{A(j)}$ = molar flow rate in anode flow channel at differential element j
 $F_{C(j)}$ = molar flow rate in cathode flow channel at differential element j
 $i_{(j)}$ = current in reactor element j
 k_m = mass transport coefficient for diffusive water transport between differential elements
 N_{SO_3} = sulfonic acid density ($1.8 \times 10^{-3}/\text{cm}^2$)
 P^w = water vapor pressure at reactor temperature T
 $P_{O_2(j)}$ = partial pressure of oxygen in cathode flow channel element j
 $P_{H_2(j)}$ = partial pressure of hydrogen in anode flow channel element j
 $P_{w(j)}$ = partial pressure of water in element j
 P_{atm} = total pressure in the gas flow channels, atmospheric pressure
 R = gas constant
 R_L = external load resistance
 $R_{M(j)}$ = membrane resistance in element j
 T = fuel cell reactor temperature
 V_A = volume of anode flow channel in a differential element of the reactor

V_C = volume of cathode flow channel in a differential element of the reactor

$V_{FC(j)}$ = battery voltage in differential element j

$\lambda_{(j)}$ = number of water molecules per sulfonic acid residue in the membrane

References and Notes

- (1) Larminie, J.; Dicks, A. *Fuel Cell Systems Explained*, 2nd ed.; Wiley: New York, 2003.
- (2) Barbir, F. *PEM Fuel Cells: Theory and Practice*; Elsevier Academic Press: Burlington, MA, 2005; p 433.
- (3) Martin, A. In *What we Have Learned from Vehicle Demonstration Programs?* Ninth Grove Fuel Cell Symposium, London, U.K., October 4–6, 2005; Elsevier: London, U.K., 2005.
- (4) Fronk, M. In *Fuel Cell Vehicle Commercialisation*. Ninth Grove Fuel Cell Symposium, London, U.K., October 4–6, 2005; Elsevier: London, U.K., 2005.
- (5) Moxley, J. F.; Tulyani, S.; Benziger, J. B. *Chem. Eng. Sci.* **2003**, *58*, 4705–4708.
- (6) Chia, E. S. J.; Benziger, J. B.; Kevrekidis, I. G. *AIChE J.* **2004**, *50*, 2320–2324.
- (7) Kapral, R.; Showalter, K. *Chemical Waves and Patterns*; Kluwer Academic Publishers: Boston, MA, 1995; Vol. 10, p 640.
- (8) Epstein, I. A.; Pojman, J. A. *An Introduction to Nonlinear Chemical Dynamics: Oscillations, Waves, Patterns and Chaos*; Oxford University Press: New York, 1998; p 408.
- (9) Luss, D. *Ind. Eng. Chem. Res.* **1997**, *36*, 2931–2944.
- (10) Luss, D.; Sheintuch, M. *Catal. Today* **2005**, *105*, 254–274.
- (11) Marwaha, B.; Sundarram, S.; Luss, D. *Chem. Eng. Sci.* **2004**, *59*, 5569–5574.
- (12) Marwaha, B.; Sundarram, S.; Luss, D. *J. Phys. Chem. B* **2004**, *108*, 14470–14476.
- (13) Benziger, J.; Chia, E.; Karnas, E.; Moxley, J.; Teuscher, C.; Kevrekidis, I. G. *AIChE J.* **2004**, *50*, 1889–1900.
- (14) Benziger, J.; Chia, E.; Moxley, J. F.; Kevrekidis, I. G. *Chem. Eng. Sci.* **2005**, *60*, 1743–1759.
- (15) Berg, P.; Promislow, K.; St Pierre, J.; Stumper, J.; Wetton, B. *J. Electrochem. Soc.* **2004**, *151*, A341–A353.
- (16) Dutta, S.; Shimpalee, S.; Van Zee, J. W. *J. Appl. Electrochem.* **2000**, *30*, 135–146.
- (17) Lee, W. K.; Shimpalee, S.; Van Zee, J. W. *J. Electrochem. Soc.* **2003**, *150*, A341–A348.
- (18) Raistrick, I. D. Electrode Assembly for Use in a Solid Polymer Electrolyte Fuel Cell. U.S. Patent 4876115, October 24, 1989. Assignee, U.S. Dept. of Energy.
- (19) Yang, C.; Srinivasan, S.; Bocarsly, A. B.; Tulyani, S.; Benziger, J. B. *J. Membr. Sci.* **2004**, *237*, 145–161.